Aerobic Partial Oxidation of Alkanes using Photo-driven Iron Catalysis

Nathan Coutard,[1] Jonathan M. Goldberg,[2] Henry U. Valle,[2] Yuan Cao,[2] Xiaofan Jia,[1] Philip D. Jeffrey,[3] T. Brent Gunnoe,[1*] John T. Groves[2*]

[1]Department of Chemistry, University of Virginia, Charlottesville, Virginia 22904, United States
[2]Department of Chemistry, Princeton University, Princeton, New Jersey 08544, United States
[3]Department of Molecular Biology, Princeton University, Princeton, New Jersey 08544, United States

tbg7h@virginia.edu
jtgroves@princeton.edu

Abstract

Photo-driven oxidations of alkanes in trifluoroacetic acid using commercial and synthesized Fe^{III} sources as catalyst precursors and dioxygen as the terminal oxidant are reported. The reactions produce alkyl esters, occur at ambient temperature in the presence of air, and catalytic turnover is observed for the oxidation of methane in a pure dioxygen atmosphere. Under optimized conditions, approximately 17% conversion of methane to methyl trifluoroacetate at more than 50% selectivity is observed. It is demonstrated that methyl trifluoroacetate is stable under catalytic conditions, and, thus, over-oxidized products are not formed through secondary oxidation of methyl trifluoroacetate.

Introduction

There is great interest in the fundamental chemistry of hydrocarbon partial oxidation via C–H bond activation using dioxygen as the terminal oxidant. However, despite extensive research, the selective partial oxidation of alkanes stands among the most challenging chemical reactions.[1] The high bond dissociation energy of alkane C–H bonds (typically > 96 kcal/mol) combined with the often weaker C–H bonds of functionalized products frequently leads to cascading oxidation reactions and undesirable overoxidation, including the production of carbon dioxide.[2] As a result, current industrial processes for the production of methanol from methane rely on an indirect route involving the conversion of methane to synthesis gas (i.e., syngas, CO/H_2), which is energy and capital intensive.[3] Hence, there is motivation for new processes for the direct partial oxidation of alkanes under ambient conditions.[4] While examples of thermal alkane partial oxidation using transition metals have been reported, many of them either have not been tested for light alkanes,[5] yield over-oxidized products,[6] require complex catalysts and/or multi-step and energy-intense extraction procedures,[6a, 7] or make use of terminal oxidants not recycled by dioxygen, preventing industrial viability.[8]

The Catalytica process, which uses a Pt(II) catalyst in oleum, stands out as it provides high selectivity and conversion of methane to methylbisulfate, which can be hydrolyzed to form methanol.[9] Catalytic conversion of methane to methylbisulfate has been demonstrated for other electrophilic catalysts [i.e., in addition to Pt(II)] in superacidic media.[10] However, drawbacks of such processes include the susceptibility of the electrophilic metal center to poisoning by even strong acids and the energy intensive process required to separate methyl bisulfate from oleum.

Recently, there has been growing interest in photo-driven C–H functionalization with some advancements on strategies for C–C coupling.[11] Photochemistry can allow the selective formation of high-energy intermediates that cannot be obtained thermally. However, there is little precedent regarding photolytic conversion of light alkanes, and only a few publications report the oxidation of non-functionalized alkanes using photocatalysis. Turnovers are attained for conversion of light alkanes to tert-butoxycarbonyl-protected hydrazines using cerium chloride photocatalysts.[12] Selective conversion of methane to methanol using a TiO_2 supported Fe catalyst and H_2O_2 as a terminal oxidant was reported,[13] as well as aqueous photo-oxidation of methane to methanol with perrhenate salts.[14] Previously, our groups have reported oxy-esterification of light alkanes in trifluoroacetic acid (HTFA), in both thermal and photolytic processes,[15a-d] and the groups of Goldberg and Schelter have reported an aerobic photocatalytic process for alkane iodination.[15e]

Results and discussion

We screened a series of commercial, air-stable Fe^{III} compounds for alkane photo-oxidation. For these initial screens, we used reactions that are stoichiometric in Fe^{III}. Iron 1,3,5-benzenetricarboxylate (Fe-BTC) and $[Et_4N]FeCl_4$ previously have been shown to functionalize C–H bonds of cyclohexane and toluene in organic solvents under photochemical conditions in the presence of an external oxidant (air/O_2).[16] For our initial screening, Fe^{III} compounds (0.25 mmol) were combined with HTFA and cyclohexane (1.25 mmol), and the mixture was irradiated with a 370 nm LED for 24 h (Table 1). Of the Fe compounds we examined, commercial Fe^{III} trifluoromethanesulfonate ($Fe(OTf)_3$) performed the best, giving a quantitative yield of cyclohexyl-trifluoroacetate (Cy-TFA), based on amount of Fe^{III}, with no detectable overoxidation (e.g., cyclohexanone or difunctionalized products). The quantitative yield based on Fe^{III} is the theoretical maximum for a two-electron reaction, assuming that two Fe^{III} centers are required for conversion of cyclohexane and HTFA to Cy-TFA (note: these initial screening reactions were stoichiometric in Fe^{III}). The quantum yield for this process was determined to be ~1% using standard iron oxalate actinometry, although this value is certainly an underestimate due to the turbidity of the reaction mixture (see Supporting Information). $Fe(acac)_3$ (acac = acetylacetonate), which contains three bidentate κ^2-*O*,*O* acac ligands, gave moderate functionalization with only 26% yield over the same time period. We hypothesize that the bidentate acac ligands are bound too strongly to allow full conversion to the proposed active Fe species that is responsible for C–H functionalization over the time allowed for the reaction (24 hours, *vide infra*). LEDs can generate heat, resulting in the reactors reaching temperatures of 40-50 °C. In a control experiment performed in the dark for 24 h at 60 °C, no cyclohexane functionalization was detected, demonstrating the photochemical nature of the reaction.

Table 1. Screening of Fe^{III} compounds for photochemical cyclohexane functionalization.[a]

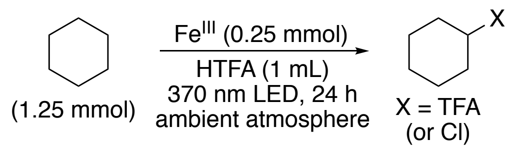

Entry	Fe^{III} Source	Yield f(n_{Fe})
1	None	ND
2	None (0.75 mmol HOTf)	ND
3	Fe_2O_3	trace
4[b]	Fe_3O_4	<1%
5[c]	$Fe(acac)_3$	26%
6	$[Et_4N]FeCl_4$	100% [d,e]
7[c]	Fe-BTC	96%
8	$Fe(OTf)_3$	100%
9[f]	$Fe(OTf)_3$	18%

[a] Yields based on the amount of iron, abbreviated yield f(n_{Fe}), are determined by GC-MS vs. tetradecane as an internal standard and are the average of two experiments. [b] Both Fe_2O_3 and Fe_3O_4 are only partially soluble in TFA, affording inactive Fe_3-μ_3O upon dissolution (see below). For Fe_3O_4 0.26 mmol was used. Yield based on equiv of Fe_3O_4 and does not account for reaction stoichiometry in (a). [c] Detected < 5% cyclohexyl-1,2-TFA. [d] Cyclohexyl-TFA 18%, cyclohexyl-Cl 82%. [e] Trace cyclohexanone detected. [f] Blue LED (400-500 nm) used instead of 370 nm. ND = not detected.

With these promising results selectively activating a single C–H bond in cyclohexane, the scope of substrates was expanded to other alkanes. C–H functionalization was observed using $Fe(OTf)_3$ for methane, ethane, propane, cyclopentane and *n*-pentane (Table 2). Yields against n_{Fe} are 60% for MeTFA, 36% for EtTFA and the combined yield for propane oxidation products reached ~2 turnovers (TOs). For all substrates, the TFA mono-ester was the major product. In the case of propane, preference for the 2-propyl trifluoroacetate over the 1-propyl trifluoroacetate in an approximate 2:1 ratio is consistent with a process involving net homolytic H atom abstraction, selecting for the weaker internal C–H bond over the stronger terminal C–H bond.[15a, 15d] While the difference in yields between methane, ethane and propane cannot be directly correlated to the strength of the C–H bonds, similar observations were reported for the photo-amination of light alkanes by cerium salts, with the solubility of different alkanes impacting reaction yields.[12] The observation of CHF_3 and CHF_2TFA for some reactions is discussed below.

Table 2. Screening substrates for photo-oxidation using $Fe(OTf)_3$ in HTFA.

$$\text{alkane} \xrightarrow[\substack{\text{HTFA} \\ \text{370 nm LED, 24 h} \\ \text{ambient atmosphere}}]{Fe(OTf)_3\ (0.25\ \text{mmol})} \text{product(s)}$$

Entry	Alkane	Product(s)	Yield f(n_{Fe})
1[a]	CH_4	CH_3TFA	60 ± 4%
2[a]	C_2H_6		36 ± 2%
		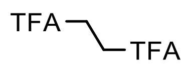	ND
3[a]	C_3H_8	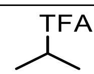	140 ± 24%
		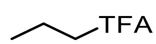	64 ± 14%
		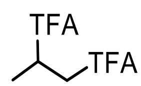	ND
4[b]	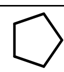	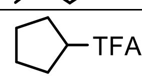	50%
5[b]	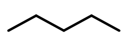	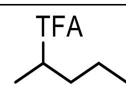	52%
		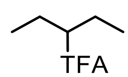	30%
6[b]	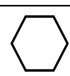	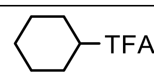	100%
7[b]	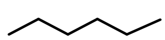	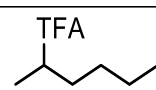	56%
		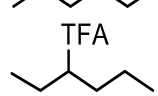	34%

[a] Alkane (gaseous, 100 psig), HTFA (8 mL), 90 mL Fisher-Porter pressure reaction vessel. [b] Alkane (liquid, 1.25 mmol), HTFA (1 mL), 8 mL microwave vial with crimp cap. Yields averaged from [a] three or [b] two experiments, measured by [a] NMR or [b] GC-MS. ND = not detected. Typical NMR or GC-MS spectra for the characterization of products for each of the above reactions can be found in the Supporting Information for all substrates: methane (Figure S9), ethane (Figure S10), propane (Figure S11), and liquid alkanes (Figures S15 through S18). The observation of CHF_3 and CHF_2TFA is discussed below.

Combining each of the active Fe compounds in Table 1 with alkanes in HTFA results in heterogeneous mixtures. After removal of the solids by filtration, the soluble fractions gave the same absorbance feature in UV-Vis spectra at ~340 nm (Figure S1). This common feature suggests *in situ* formation of the same soluble Fe species. In separate experiments, we monitored the formation of Cy-TFA over time using $Fe(OTf)_3$ and $Fe(TFA)_3$ as Fe^{III} sources (Figure 1). Both reactions give near-quantitative formation of Cy-TFA after 24 h of photolysis. When using $Fe(OTf)_3$, an induction period followed by rapid formation of Cy-TFA was observed, while the $Fe(TFA)_3$ plot appears approximately linear, suggesting that Fe^{III} salts initially undergo a reaction with the HTFA solvent to form an Fe^{III} complex that mediates alkane oxidation. The relatively poor activity of $Fe(acac)_3$ compared to complexes (see above) with more labile ligands is consistent with the strong coordination of acetylacetonate.

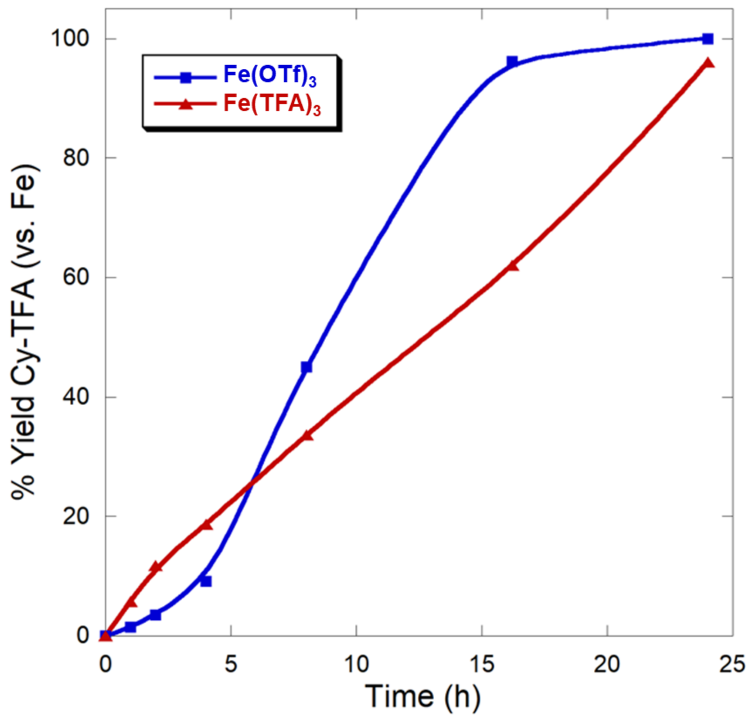

Figure 1. Cy-TFA production by photolysis of Fe^{III}/HTFA mixtures with a 370 nm LED. Each point on the plot resulted from a separate reaction. The lines are added to guide the eye. 0.25 mmol Fe^{III}, 1.25 mmol cyclohexane, 1 mL HTFA, 8 mL microwave vial with crimp cap. The photoreduction of Fe^{III} to Fe^{II} followed a similar time course (Figure S19).

In excess HTFA, the Fe^{III} salts react to form $Fe^{III}_x(TFA)_y$ clusters.[17] A previous report showed that refluxing anhydrous $Fe^{III}Cl_3$ in HTFA leads to formation of a hygroscopic white solid described as "$Fe(TFA)_3$."[18] Upon exposure to moisture, this white solid changes color to form a red material, the structure of which was later reported.[19] We were able to crystallize a similar structure (CCDC 2096583, Figure S2, Tables S1 through S9) as $[Fe^{III}_3(\mu_3\text{-O})(H_2O)_2(\mu\text{–TFA})_6(TFA)](HTFA)$, termed "$Fe_3$-$\mu_3$O" herein. The structure shows three Fe(III) ions are arranged around a central μ_3 bridging oxo coplanar with three Fe^{III} atoms. Two of the Fe atoms have water molecules coordinated trans to the μ_3-oxo bridge and have short Fe-oxo bond distances (1.912(2) Å). The third iron-oxo bond distance is longer (1.955 Å), reflecting the trans-trifluoroacetate ion on that Fe. Although the structure we determined for

$[Fe^{III}_3(\mu_3\text{-}O)(H_2O)_2(\mu\text{–}TFA)_6(TFA)](HTFA)$ is similar to the previously reported structure,[19] one of the protons in the aqua ligands in the structure is resolved and involved in a hydrogen bond with a disorganized solvent molecule rather than with the fluorine of a clearly defined TFA ligand. $Fe_3\text{-}\mu_3O$ was further characterized using Mössbauer and EPR spectroscopy (Figures S13 and S14), which show characteristics typical of high-spin ferric iron.

We studied the effect of dioxygen and water on methane oxidation using freshly prepared anhydrous $Fe(TFA)_3$ handled in an anaerobic environment (Table 3). While dioxygen was required to oxidize methane to MeTFA using $Fe(TFA)_3$, the presence of water was detrimental to activity. For example, adding 2 equiv (relative to the amount of $Fe(TFA)_3$) of H_2O under 1 atm of dry dioxygen reduced the MeTFA yield from ~200% (i.e., two catalytic turnovers) to 34% (Entries 2 and 3, Table 3). Adding 22 equiv of water rendered $Fe(TFA)_3$ entirely inactive (Entry 6, Table 3). These results indicate that the active species for alkane oxidation is not the $Fe_3\text{-}\mu_3O$ complex. Thus, we propose that $Fe(TFA)_3$ is the active species for hydrocarbon oxidation, but can react with water to form the inactive $Fe_3\text{-}\mu_3O$ complex. Thus, under aerobic conditions, as the hydrocarbon is oxidized and water is formed, inhibition of catalysis is anticipated (Scheme 1).

Table 3. Screen of conditions for methane oxidation with $Fe(TFA)_3$.[a]

$$\underset{(100\ \text{psig})}{CH_4} \xrightarrow[\substack{\text{HTFA (8 mL)} \\ \text{370 nm LED, 24 h}}]{\substack{\text{"}Fe(TFA)_3\text{" (0.25 mmol)} \\ \pm\ H_2O\ \text{(0.5 or 5.5 mmol)} \\ \pm\ O_2\ \text{(1 atm)}}} \text{MeTFA}$$

Entry	O_2	H_2O	Yield f(n_{Fe})
1	Reaction carried in air		33 ± 2%
2[b]	+	+	34 ± 5%
3[c]	+	-	196 ± 13%
4[b]	-	+	trace
5[c]	-	-	ND
6[d]	+	++	ND

[a] Standard reaction conditions: 0.25 mmol $Fe(TFA)_3$, 100 psig CH_4, 8 mL HTFA, 370 nm LED, 90 mL Fisher-Porter pressure reaction vessel. Yields were determined by ^1H NMR spectroscopy with CH_3NO_2 as internal standard. HTFA and H_2O were degassed with N_2. Yields are averaged from triplicate experiments. ND = not detected, trace = yield < 1%. [b] 0.5 mmol H_2O added [c] To remove all water, reaction carried in 8 mL of HTFA:TFAA in 4:1 vol. ratio. TFAA is trifluoroacetic anhydride. [d] 5.5 mmol H_2O added.

$$CH_4 + {}^1/_2\, O_2 + \text{HTFA} \xrightarrow{\text{cat. } Fe(TFA)_3} CH_3TFA + H_2O$$

$$3\ Fe(TFA)_3 + 3\ H_2O \xrightarrow{-\ \text{HTFA}} [Fe^{III}_3(\mu_3\text{-}O)(H_2O)_2(\mu\text{-}TFA)_6(TFA)](HTFA)$$

Scheme 1. Oxidation of methane by dioxygen in HTFA, followed by formation of the inactive $[Fe^{III}_3(\mu_3\text{-}O)(H_2O)_2(\mu\text{–}TFA)_6(TFA)](HTFA)$, through reaction of $Fe(TFA)_3$ with H_2O.

The hypothesis that an inactive species is formed in the presence of water is supported by UV-Vis characterization of $Fe(TFA)_3$ in different solvent mixtures (Figure 2). $Fe(TFA)_3$ is insoluble in rigorously dry HTFA and gives no discernible features in the UV-Vis spectrum. Upon addition of water, red $Fe_3\text{-}\mu_3O$ is formed, characterized by an absorption at 338 nm. $Fe(TFA)_3$ is soluble in dry acetonitrile with characteristic absorption features at 313 and 359 nm. The addition of water makes these features disappear with the concomitant appearance of the characteristic Fe_3-μ_3O feature at 338 nm.

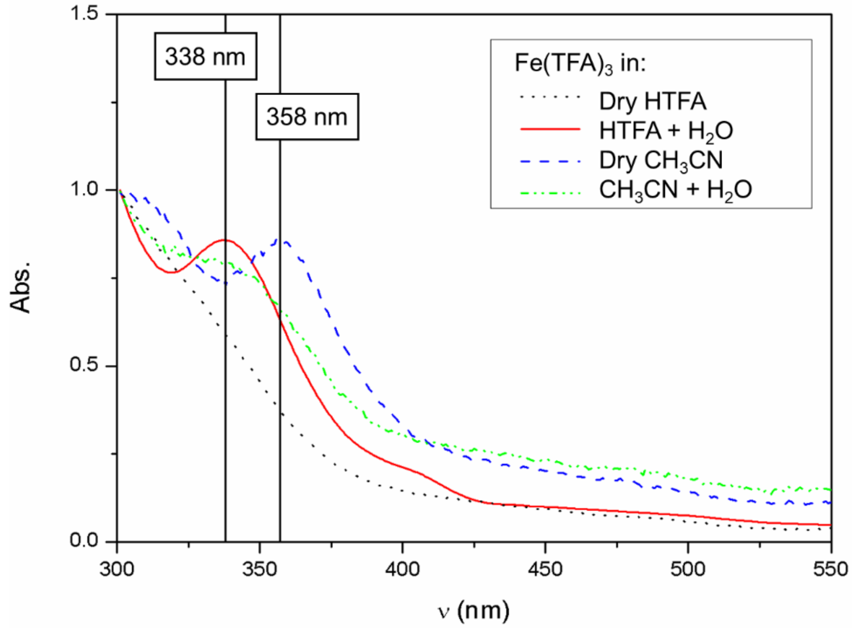

Figure 2. UV-Vis spectra of $Fe(TFA)_3$ in dry HTFA, HTFA:H_2O mixture (20:1 ratio by volume), dry CH_3CN and CH_3CN:H_2O mixture (20:1 ratio by volume).

Since water is an expected by-product of methane oxidation using O_2, we added trifluoroacetic anhydride (TFAA) to a methane photo-oxidation reaction to trap by-produced water before it could poison the catalyst. Under these conditions, the amount of MeTFA formed is a direct function of n_{O2} ($n_{MeTFA} = 0.14 \pm 0.01\ n_{O2}$), supporting the role of dioxygen as the terminal oxidant (Figure S3). With a large excess of dioxygen, up to 24 TOs of MeTFA and ~17% conversion of methane could be obtained (Scheme 2). High methane conversion could not be reached at high turnover, which we attribute to the degradation of $Fe(TFA)_3$ as it likely oxidizes the solvent at lower methane concentrations.

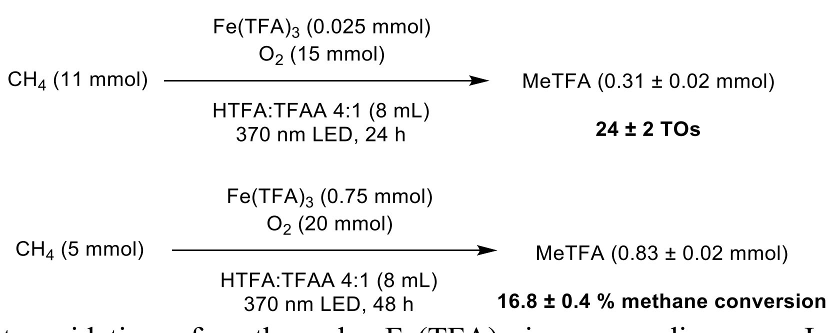

Scheme 2. Photo-oxidation of methane by $Fe(TFA)_3$ in excess dioxygen. In the absence of $Fe(TFA)_3$, MeTFA is not observed. Where TOs are measured, we assume two equiv of Fe^{III} are required for each conversion of methane and HTFA to MeTFA. Standard deviations based on a minimum of three independent experiments.

A key challenge for the selective partial oxidation of light alkanes is over oxidation, which is often a result of the intrinsically high reactivity of functionalized alkyl products compared with starting alkanes. To determine the potential efficacy of Fe-catalyzed photo-driven hydrocarbon partial oxidation, we compared the rate of MeTFA formation from methane to the rate of MeTFA consumption under reaction conditions. The degradation rate of MeTFA under reaction conditions was assessed and shown to be much slower than the rate of its formation, with > 90% MeTFA remaining after 24 h (Figure 3). Regardless of the mechanism for the formation of MeTFA, the mono oxidized product is stable under reaction conditions, indicating a protective effect of the ester moiety.[15] Under the conditions in Figure 3, the different solubilities of methane and MeTFA play a role. While methane oxidation proceeds under ideal conditions (before substrate depletion or catalyst decomposition), the rate of MeTFA formation is ~ 16 times faster than the rate of MeTFA degradation. Hence, any significant CO_2 production does not likely originate from overoxidation of MeTFA, demonstrating the viability of high selectivity at high conversion of methane.

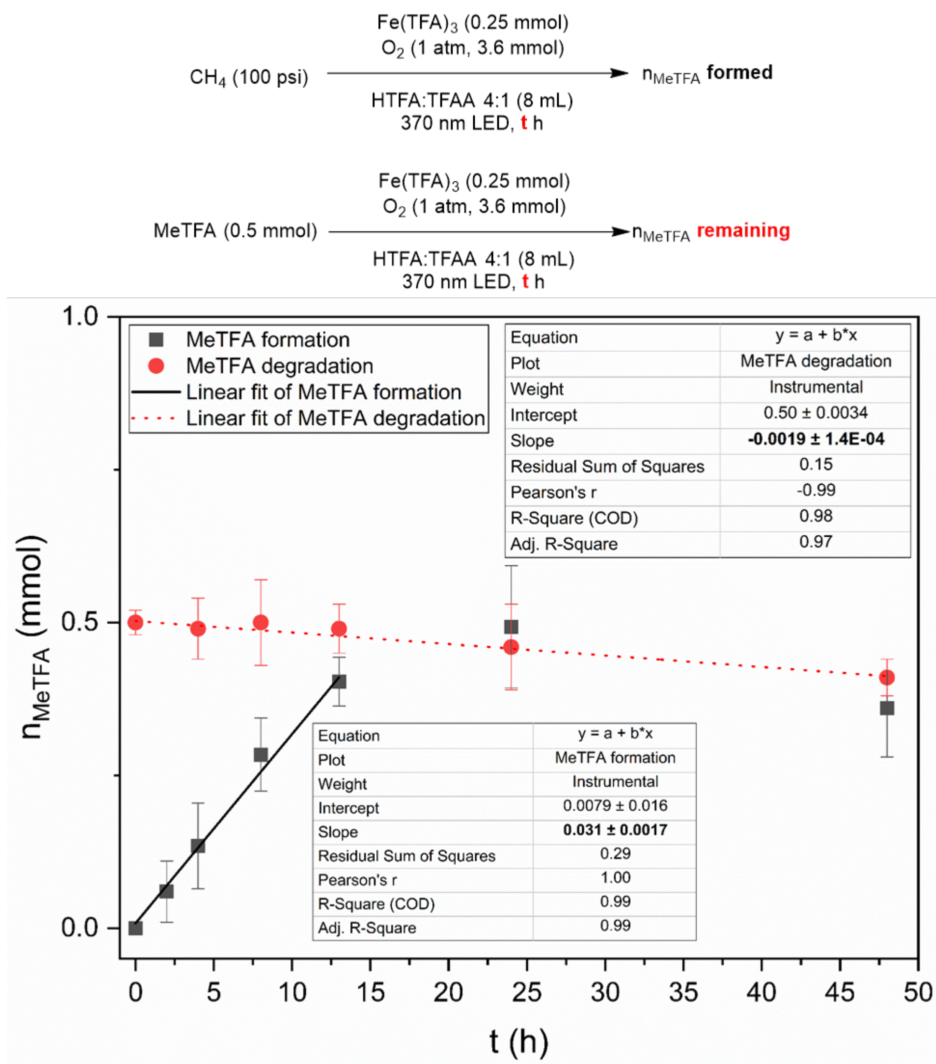

Figure 3. Rate of formation (black squares) and degradation (red dots) of MeTFA under photolytic conditions (see equations above plot for conditions). Data for MeTFA degradation are fitted linearly between 0 h and 48 h, data for MeTFA formation are fitted between 0 h and 12 h.

A pressurized J-Young NMR tube was used to observe gaseous, proton-containing by-products. Upon photolysis of $Fe(TFA)_3$ in HTFA with 50 psig of methane, we detected difluoromethyl trifluoroacetate ($CHF_2CO_2CF_3$, δ = 6.91 ppm, triplet, $^2J_{HF}$ = 70 Hz) and trace trifluoromethane (CHF_3, δ = 6.18 ppm, quartet, $^2J_{HF}$ = 80 Hz),[20] both of which are known HTFA degradation products (Figure 4).[21] Replacing the methane with Ar, both $CHF_2CO_2CF_3$ and CHF_3 were observed, but formation of MeTFA was not detected (Figure 4). Furthermore, upon replacing HTFA with deuterated trifluoroacetic acid (DTFA), only trace $CHF_2CO_2CF_3$ and CHF_3 were observed under either Ar or CH_4 atmosphere. Under these conditions, the formation of small amounts of $CHF_2CO_2CF_3$ and CHF_3 likely arise from trace protio-HTFA remaining in DTFA. These observations point to HTFA degradation, and not that of methane, as the origin of these by-products. This was also observed for the oxidation of substrates with weaker C–H bonds than that of methane, such as propane (Figure S4) and cyclohexane (Figure S12) in DTFA/TFAA. However, CHF_3 formation during the oxidation of cyclohexane was observed even in DTFA/TFAA, pointing to the more reactive nature of the cyclohexane C–H bond compared to that of lighter alkanes, and the consequent ability of a CF_3 radical to abstract this hydrogen atom.

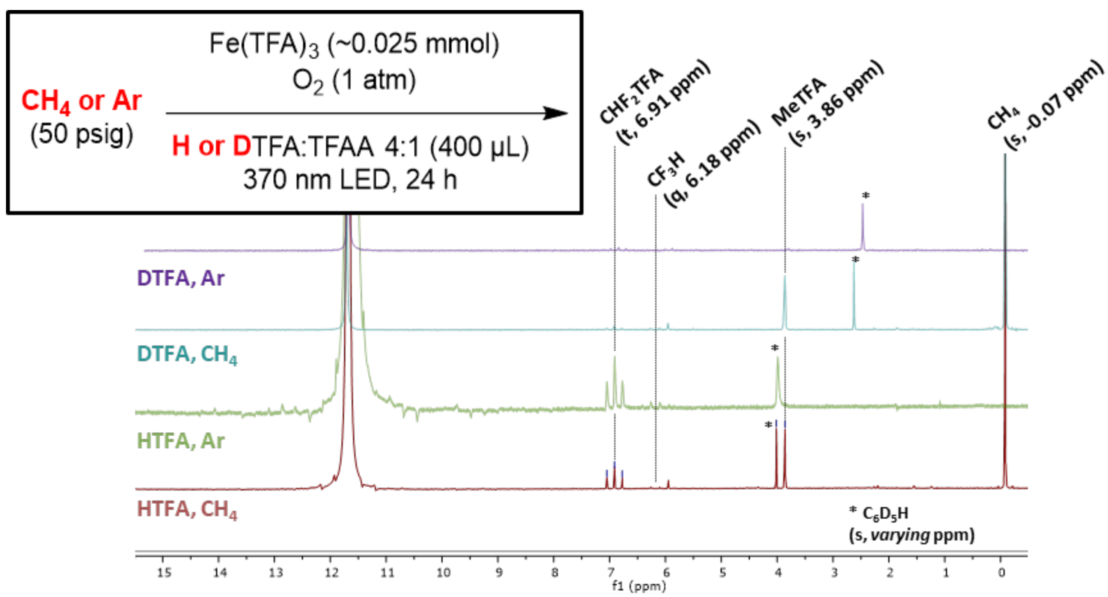

Figure 4. 500 MHz ^{1}H NMR spectra resulting from the illumination of $Fe(TFA)_3$ with a 370 nm LED light under different conditions of solvent and headspace. A C_6D_6 capillary was used as a locking solvent for the NMR. The signal of the residual C_6D_5H signal for the lock solvent is observed at unpredictable shift values due to paramagnetic shifts of the reaction media, which does not shift the C_6D_5H signal in the sealed capillary. Use of a coaxial NMR tube insert did not fix this variability. The addition of tetramethylsilane (TMS) to the capillary tube showed consistent separation of C_6D_5H and TMS peaks, with both signals shifted from peaks arising from the reaction mixture (Figure S12). Spectra are hence referenced using either CH_4 (s, -0.07 ppm) or CHF_2TFA (t, 6.91 ppm).

Gaseous by-products were quantified at 17% conversion of methane to MeTFA through headspace analysis using a GC-TCD. Trace CO (< 0.1% yield) was observed, however no ethane or ethylene was detected. Evidence of CO_2 formation was obtained in the headspace of reactions with either CH_4 or Ar (without CH_4), leading to the conclusion that part of the CO_2 was a product of solvent oxidation (HTFA) rather than methane overoxidation (Figures S5, S7). Labelled $^{13}CH_4$ allowed us to assess the quantity of CO_2 arising from methane overoxidation through GC-MS (Figure S8). At 14% conversion of $^{13}CH_4$ to ^{13}MeTFA, selectivity for ^{13}MeTFA was 56%, the remainder being 44% $^{13}CO_2$ and trace (<0.1%) CO. Because of the stability of MeTFA under reaction conditions (Figure 3), we believe that CO_2 does not come from the oxidation of MeTFA but is rather formed by a different, and unknown, reaction pathway, possibly degradation of a reactive intermediate species. This is encouraging when considering the possible use of differently coordinated Fe^{III} or other transition metal photo-catalysts to improve selectivity.

Summary and Conclusions

We report here new reactivity for several commercial Fe^{III} salts for the photo-oxidation of a variety of linear and cyclic alkanes, C1 to C6. From our initial observations, we concluded that a range of Fe^{III} sources soluble in HTFA converged toward a common pathway, leading us to investigate a likely formed complex, $Fe(TFA)_3$, as the active species. We found this complex active for the oxidation of methane, and we characterized a poisoned state of the catalyst that arose from reaction of the active species with water. As water is an expected by-product of alkane oxidation, we developed conditions that remove the water as the reaction proceeded and observed catalytic turnover for the oxidation of methane to MeTFA. Notably dioxygen was determined to be the terminal oxidant, and 17% conversion of methane to the mono-ester product was attained at more than 50% selectivity.

Experimental Methods

Caution! Many of the reagents and conditions described herein are hazardous. Trifluoroacetic acid (HTFA) is highly corrosive and should be handled inside a fume hood with long nitrile gloves covering up to the elbow. LED lamps produce high intensity UV light and direct eye or skin contact should be avoided. Appropriate safety procedures should be consulted prior to handling concentrated acids, strong oxidants, and mixtures of hydrocarbon substrates and O_2.

General considerations. All reactions were carried out under ambient atmosphere unless otherwise stated. HTFA, cyclohexane, chlorocyclohexane, anhydrous $FeCl_3$, Fe_2O_3, Fe_3O_4, $Fe(acac)_3$, $[Et_4N]FeCl_4$, Fe-BTC, and $Fe(OTf)_3$, tetradecane, *tert*-butanol, were purchased from commercial sources and used as received. PTFE filters (0.45µm) were purchased from Fisher. Dioxygen (99.6% purity) was purchased from Sigma Aldrich and used as received. Authentic cyclohexyl-trifluoroacetate (Cy-TFA) and 1,2-bis(trifluoroacetoxy)-cyclohexane were prepared according to a published procedure.[22] $Fe(TFA)_3$ and $Fe(TFA)_3 \bullet xH_2O$ were prepared according to published procedures with a slight modification to include Apiezon PFPE 501 as the grease used to connect the round bottom flask to the reflux condenser.[18] Microwave vials were purchased from Biotage and used as received. Teflon stoppered flasks (10 mL) were purchased from Chemglass and used as received. The 370 nm LED is a Kessil PR160-370 40 W LED and was used as received. The blue LED (400-500 nm) is a Kessil H150-blue 30 W High Luminous DEX 2100 LED and was used as received. GC-MS analysis was performed using an Agilent Technologies 7890A gas chromatograph equipped with a fused silica column (crossbond 35% diphenyl-65% dimethyl polysiloxane; 30 m × 0.32 mm; 0.5 µm thickness) and electron impact mass analyzer. GC-TCD analysis was conducted in a Shimadzu GC-2014. UV-Vis spectral measurements were recorded on an Agilent 8453 diode array spectrophotometer at room temperature, with a 1 cm path length quartz cuvette. Zero-field ^{57}Fe Mössbauer spectra were recorded on a SEE Co. Mössbauer spectrometer (MS4) at 80 K in constant acceleration mode. ^{57}Co/Rh was used as the radiation source. WMOSS software was used for the quantitative evaluation of the spectral parameters (least-squares fitting to Lorentzian peaks). The temperature of the sample was controlled by a Janis Research Co. CCS-850 He/N2 cryostat within an accuracy of 0.3 K. Isomer shifts were determined relative to α-iron at 298 K. EPR was recorded on a Bruker EPR EMX Plus. NMR spectra were recorded on a Varian Inova 500 MHz spectrometer.

Photochemical functionalization of gaseous light alkanes by Fe(III) compounds. A 90 mL glass Fisher-Porter reactor was charged with a stir bar, 0.25 mmol of an Fe(III) source and HTFA (8 mL, 104.5 mmol). The reactor was then sealed and pressurized with alkane (methane, ethane or propane) at 100 psig. The reactors were placed on a stir plate and irradiated with either a mercury lamp (Hanovia medium pressure UV lamp, 450 W, Ace Glass) or two 370 nm LED lamps (Kessil PR-370). Following the reaction, the lamp(s) was turned off, and the reactor was vented in a Tedlar sampling bag to keep for headspace analysis. For analyzing the liquid phase, internal standard, either CH_3NO_2 or HOAc, was added to the reaction mixture in a known concentration to allow for quantification of products. An aliquot was removed for centrifugation, and the supernatant was used for ^{1}H NMR analysis, following a previously published procedure from our laboratory.[15a, 15b] Unless otherwise mentioned, reactions were carried out in air. When air was excluded, the reactors were charged using a N_2 glove box and Schlenk line using N_2 degassed HTFA. When needed, dry O_2 was added by bubbling the vessel for 10 minutes. When needed, N_2-degassed H_2O was added through cannula transfer from a N_2-purged Schlenk flask. Representative ^{1}H NMR spectra resultant from the oxidation of methane, ethane and propane are shown in Figures S9, S10 and S11 respectively.

Photochemical functionalization of liquid alkanes by Fe(III) compounds. Under ambient atmosphere, an 8 mL microwave vial was charged with an Fe(III) source (0.25 mmol) and a stir bar. HTFA (1 mL) and liquid alkane (1.25 mmol) were added to the vial. The vial was sealed with a crimp cap containing a septum. The vial was placed ~5 cm in front of a 370 nm LED (unless otherwise stated) and allowed to stir for 24 h. The reaction mixture was removed from the vial and filtered through a PTFE filter into a vial containing tetradecane (0.13 mmol). The reaction vial was rinsed with dichloromethane (5 mL) and filtered. The solutions were combined and washed two times with 10 mL H_2O. The organic layer was eluted through a small silica plug to remove any trace Fe and then dried over $MgSO_4$. An aliquot was taken from the dichloromethane solution and analyzed by GC-MS to quantify cyclohexyl-trifluoroacetate. Representative GC-MS data resultant from the oxidation of cyclohexane, cyclopentane, *n*-pentane, and *n*-hexane are shown in Figures S15, S16, S17 and S18 respectively.

High conversion and high turnover oxidation of methane. To demonstrate possible catalytic turnover, the amount of $Fe(TFA)_3$ was lowered to 0.025 mmol and a 4:1 mixture of HTFA:TFAA (8 mL) was used as the solvent. Then, 20 mmol of O_2 and 50 psig of methane were added and the reaction was performed for 24 hours. To reach higher conversion, the amount of $Fe(TFA)_3$ was increased to 0.75 mmol and the solvent was a 4:1 mixture of HTFA:TFAA (8 mL). Then, 15 mmol of O_2 and 50 psig of methane were added and the reaction time was extended to 48 hours.

Photochemical functionalization of alkanes in J-Young NMR tubes. A J-Young NMR tube was charged with a capillary tube containing C_6D_6, 10 mg of $Fe(TFA)_3$ and a 4:1 mixture of H- or D-TFA:TFAA (400 μL). The tube was then purged with pure O_2, sealed and pressurized with 50 psig of either Ar, CH_4 or C_3H_8 or 1.25 mmol of cyclohexane. The tubes were irradiated with two 370 nm LED lamps (Kessil PR-370). Following the reaction, the lamp was turned off and

NMR spectra were collected without opening the tubes to preserve the headspace pressure of side-products.

Preparation of UV-Vis samples. An Fe(III) salt (0.25 mmol Fe) was combined with HTFA (1 mL) and cyclohexane (135 µL, 1.25 mmol), unless otherwise stated, to give a yellow/red mixture. The mixture was filtered through a PTFE filter and diluted to optical density < 2. For samples in MeCN, a corresponding Fe(III) salt was combined with MeCN (1 mL), filtered through a PTFE filter and diluted to OD < 2.

Headspace analysis. After a reaction reached completion, the headspace of the reactors was depressurized in a Tedlar sampling bag, which was kept at -36 °C in a freezer until analysis of the sample. Analysis was conducted in a Shimadzu GC-2014 equipped with a TCD detector by flushing a 500 µL injection loop with 1 mL of the gas headspace. The sample is first passed through a 1.0 m Hayesep T 80/100 column to trap solvent residue and moisture, then through a 1.5 m Hayesep Q 80/100 and 2.0 m MS5A 60/80 molecular sieve column using a custom dual valve setup. The detector temperature was 200 °C, the current was 100 mA and the column temperature was 75 °C. Injector temperature was 68 °C. A typical GC-TCD trace for the oxidation of methane with $Fe(TFA)_3$ is shown in Figure S7. The resulting integration yielded an amount of CO_2 as a volumetric fraction of total headspace, using independently measured calibration curves established from standards prepared with known volumetric fractions of CO_2 in CH_4 (Figure S6). Consistent detector response was seen when using CO_2/CH_4 mixtures or CO_2/N_2 mixtures or CO_2/O_2 mixtures, with a given % vol. of CO_2 yielding statistically identical peak integration. These volumetric fractions were then converted to an amount of substance using total headspace volume, measured by submitting the sampling bag to Archimedes' principle. To assess the isotopic ratio of $^{12}CO_2$ to $^{13}CO_2$, a portion (1 µL) of the headspace was injected in a GC/MS (Shimadzu GCMS-QP2010 Plus system with a Restek RT-Qbond 30 m × 8 mm fused silica PLOT column with 8 µm thickness using electron impact ionization). GC-MS Parameters: starting temperature: 40 °C; time at starting temp: 3 min; ramp: 20 °C/min up to 200 °C; flow rate (carrier): 3.01 mL/min (He); split ratio: 10:1; inlet temperature: 200 °C; detector ion source temperature: 200 °C, interface temperature: 230 °C. The CO_2 peak eluted at 2.97 min.

Sample preparation for Low Temp EPR Analysis. EPR spectra were recorded on a Bruker EMX Plus spectrometer. Crystalline powders of $[Fe^{III}_3(\mu_3\text{-O})(H_2O)_2(\mu\text{–TFA})_6(TFA)](HTFA)$ were prepared as a mixture with CH_3CN or HTFA in quartz tubes (Wilmad-LabGlass, Quartz (CFQ) EPR Tubes – 4mm OD). The temperature-dependent measurements were conducted at 10K using a continuous-flow cryostat (Oxford, ESR900) with liquid helium.

Sample preparation for zero-field ^{57}Fe Mössbauer analysis. Solid samples were sealed inside a nylon washer (0.5 inch inner diameter; 0.06 inch thickness) using two pieces of Kapton® tape (3/4 inch diameter). The washer was affixed to a copper sample mount. The mount was inserted into a Janis Research Co. He/N_2 cryostat at 80 K under a counterflow of helium. The cryostat chamber was evacuated and refilled after five minutes with one atmosphere of ultra-high purity grade helium. Data collection began after the sample temperature equilibrated at 80 K.

Acknowledgements. The authors thank Dr. Jonathan Darmon at Princeton University for help with the Mössbauer spectroscopy. This research was sponsored by the U.S. Department of Energy, Office of Energy Efficiency and Renewable Energy, Advanced Manufacturing Office, under contract DE-AC05-00OR22725 with UT-Battelle, LLC.

Supporting Information

Supporting Information: Examples of NMR and UV-Vis spectra, details of the single crystal X-ray structure study, various plots of hydrocarbon conversions, details of CO_2 quantification, EPR spectra, and GC data.

References

1. (a) Stahl, S. S.; Labinger, J. A.; Bercaw, J. E., Homogeneous Oxidation of Alkanes by Electrophilic Late Transition Metals. *Angew. Chem. Int. Ed.* **1998,** *37* (16), 2180-2192; (b) Han, B.; Yang, Y.; Xu, Y.; Etim, U. J.; Qiao, K.; Xu, B.; Yan, Z., A review of the direct oxidation of methane to methanol. *Chinese Journal of Catalysis* **2016,** *37* (8), 1206-1215; (c) Horn, R.; Schlögl, R., Methane Activation by Heterogeneous Catalysis. *Catal. Lett.* **2015,** *145* (1), 23-39; (d) Webb, J. R.; Bolaño, T.; Gunnoe, T. B., Catalytic Oxy-Functionalization of Methane and Other Hydrocarbons: Fundamental Advancements and New Strategies. *ChemSusChem* **2011,** *4* (1), 37-49.
2. (a) Tang, P.; Zhu, Q.; Wu, Z.; Ma, D., Methane activation: the past and future. *Energy Environ. Sci.* **2014,** *7* (8), 2580-2591; (b) Ravi, M.; Ranocchiari, M.; van Bokhoven, J. A., The Direct Catalytic Oxidation of Methane to Methanol—A Critical Assessment. *Angew. Chem. Int. Ed.* **2017,** *56* (52), 16464-16483.
3. (a) Gunsalus, N. J.; Koppaka, A.; Park, S. H.; Bischof, S. M.; Hashiguchi, B. G.; Periana, R. A., Homogeneous Functionalization of Methane. *Chem. Rev.* **2017,** *117* (13), 8521-8573; (b) Zakaria, Z.; Kamarudin, S. K., Direct conversion technologies of methane to methanol: An overview. *Renewable and Sustainable Energy Reviews* **2016,** *65*, 250-261; (c) Schwach, P.; Pan, X.; Bao, X., Direct Conversion of Methane to Value-Added Chemicals over Heterogeneous Catalysts: Challenges and Prospects. *Chem. Rev.* **2017,** *117* (13), 8497-8520.
4. Meng, X.; Cui, X.; Rajan, N. P.; Yu, L.; Deng, D.; Bao, X., Direct Methane Conversion under Mild Condition by Thermo-, Electro-, or Photocatalysis. *Chem* **2019,** *5* (9), 2296-2325.
5. (a) Nagarjun, N.; Dhakshinamoorthy, A., Liquid phase aerobic oxidation of cyclic and linear hydrocarbons using iron metal organic frameworks as solid heterogeneous catalyst. *Molecular Catalysis* **2019,** *463*, 54-60; (b) Company, A.; Gómez, L.; Güell, M.; Ribas, X.; Luis, J. M.; Que, L.; Costas, M., Alkane Hydroxylation by a Nonheme Iron Catalyst that Challenges the Heme Paradigm for Oxygenase Action. *J. Am. Chem. Soc.* **2007,** *129* (51), 15766-15767.
6. (a) Yu, X.; De Waele, V.; Löfberg, A.; Ordomsky, V.; Khodakov, A. Y., Selective photocatalytic conversion of methane into carbon monoxide over zinc-heteropolyacid-titania nanocomposites. *Nat. Commun.* **2019,** *10* (1), 700; (b) Almquist, C. B.; Biswas, P., The photo-oxidation of cyclohexane on titanium dioxide: an investigation of competitive adsorption and its effects on product formation and selectivity. *Applied Catalysis A: General* **2001,** *214* (2), 259-271; (c) Murcia-López, S.; Villa, K.; Andreu, T.; Morante, J. R., Partial Oxidation of Methane to Methanol Using Bismuth-Based Photocatalysts. *ACS Catalysis* **2014,** *4* (9), 3013-3019.
7. (a) Baek, J.; Rungtaweevoranit, B.; Pei, X.; Park, M.; Fakra, S. C.; Liu, Y.-S.; Matheu, R.; Alshmimri, S. A.; Alshehri, S.; Trickett, C. A.; Somorjai, G. A.; Yaghi, O. M., Bioinspired Metal–Organic Framework Catalysts for Selective Methane Oxidation to Methanol. *J. Am. Chem. Soc.* **2018,** *140* (51), 18208-18216; (b) Chen, X.; Li, Y.; Pan, X.; Cortie, D.; Huang, X.; Yi, Z., Photocatalytic oxidation of methane over silver decorated zinc oxide nanocatalysts. *Nat. Commun.* **2016,** *7* (1), 12273.
8. (a) Larpent, C.; Patin, H., Oxidation of alkanes with hydrogen peroxide catalysed by iron salts or iron oxide colloids in reverse microemulsions. *J. Mol. Catal.* **1992,** *72* (3), 315-329; (b)

Kang, J.; Park, E. D., Aqueous-Phase Selective Oxidation of Methane with Oxygen over Iron Salts and Pd/C in the Presence of Hydrogen. *ChemCatChem* **2019,** *11* (17), 4247-4251; (c) Szécsényi, Á.; Li, G.; Gascon, J.; Pidko, E. A., Unraveling reaction networks behind the catalytic oxidation of methane with H_2O_2 over a mixed-metal MIL-53(Al,Fe) MOF catalyst. *Chem. Sci.* **2018,** *9* (33), 6765-6773; (d) Shul'pin, G. B.; Nizova, G. V.; Kozlov, Y. N.; Gonzalez Cuervo, L.; Süss-Fink, G., Hydrogen Peroxide Oxygenation of Alkanes Including Methane and Ethane Catalyzed by Iron Complexes in Acetonitrile. *Adv. Synth. Catal.* **2004,** *346* (2-3), 317-332; (e) Ravi, M.; van Bokhoven, J. A., Homogeneous Copper-Catalyzed Conversion of Methane to Methyl Trifluoroacetate in High Yield at Low Pressure. *ChemCatChem* **2018,** *10* (11), 2383-2386; (f) Perry, S. C.; Pangotra, D.; Vieira, L.; Csepei, L.-I.; Sieber, V.; Wang, L.; Ponce de León, C.; Walsh, F. C., Electrochemical synthesis of hydrogen peroxide from water and oxygen. *Nature Reviews Chemistry* **2019,** *3* (7), 442-458.

9. Periana, R. A.; Taube, D. J.; Gamble, S.; Taube, H.; Satoh, T.; Fujii, H., Platinum Catalysts for the High-Yield Oxidation of Methane to a Methanol Derivative. *Science* **1998,** *280* (5363), 560-564.

10. (a) Jones, C.; Taube, D.; Ziatdinov, V. R.; Periana, R. A.; Nielsen, R. J.; Oxgaard, J.; Goddard III, W. A., Selective Oxidation of Methane to Methanol Catalyzed, with C-H Activation, by Homogeneous, Cationic Gold. *Angew. Chem. Int. Ed.* **2004,** *43* (35), 4626-4629; (b) Periana, R. A.; Taube, D. J.; Evitt, E. R.; Löffler, D. G.; Wentrcek, P. R.; Voss, G.; Masuda, T., A Mercury-Catalyzed, High-Yield System for the Oxidation of Methane to Methanol. *Science* **1993,** *259* (5093), 340-343; (c) Basickes, N.; Hogan, T. E.; Sen, A., Radical-Initiated Functionalization of Methane and Ethane in Fuming Sulfuric Acid. *J. Am. Chem. Soc.* **1996,** *118* (51), 13111-13112.

11. (a) Terrett, J. A.; Cuthbertson, J. D.; Shurtleff, V. W.; MacMillan, D. W. C., Switching on elusive organometallic mechanisms with photoredox catalysis. *Nature* **2015,** *524* (7565), 330-334; (b) Yamaguchi, E.; Maejima, S.; Itoh, A., Photo-Driven Catalytic Cross-Dehydrogenative Coupling (CDC)-Type Reactions. In *Heterocycles via Cross Dehydrogenative Coupling: Synthesis and Functionalization*, Srivastava, A.; Jana, C. K., Eds. Springer Singapore: Singapore, 2019; pp 413-444; (c) Sun, Z.; Tang, B.; Liu, K. K. C.; Zhu, H. Y., Direct photochemical cross-coupling between aliphatic acids and BF_3K salts. *Chem. Commun.* **2020,** *56* (8), 1294-1297; (d) Qu, C.-H.; Song, G.-T.; Xu, J.; Yan, W.; Zhou, C.-H.; Li, H.-Y.; Chen, Z.-Z.; Xu, Z.-G., Merging Visible Light with Cross-Coupling: The Photochemical Direct C–H Difluoroalkylation of Imidazopyridines. *Org. Lett.* **2019,** *21* (20), 8169-8173.

12. Hu, A.; Guo, J.-J.; Pan, H.; Zuo, Z., Selective functionalization of methane, ethane, and higher alkanes by cerium photocatalysis. *Science* **2018,** *361* (6403), 668-672.

13. Xie, J.; Jin, R.; Li, A.; Bi, Y.; Ruan, Q.; Deng, Y.; Zhang, Y.; Yao, S.; Sankar, G.; Ma, D.; Tang, J., Highly selective oxidation of methane to methanol at ambient conditions by titanium dioxide-supported iron species. *Nature Catalysis* **2018,** *1* (11), 889-896.

14. Kunkely, H., Photooxidation of Methane to Methanol by Perrhenate in Water under Ambient Conditions. *Zeitschrift für Naturforschung B* **2013,** *68b*, 891-894.

15. (a) Liebov, N. S.; Goldberg, J. M.; Boaz, N. C.; Coutard, N.; Kalman, S. E.; Zhuang, T.; Groves, J. T.; Gunnoe, T. B., Selective Photo-Oxygenation of Light Alkanes Using Iodine Oxides and Chloride. *ChemCatChem* **2019,** *11* (20), 5045-5054; (b) Schwartz, N. A.; Boaz, N. C.; Kalman, S. E.; Zhuang, T.; Goldberg, J. M.; Fu, R.; Nielsen, R. J.; Goddard, W. A.; Groves, J. T.; Gunnoe, T. B., Mechanism of Hydrocarbon Functionalization by an Iodate/Chloride System: The Role of Ester Protection. *ACS Catalysis* **2018,** *8* (4), 3138-3149; (c) Kalman, S. E.; Munz, D.; Fortman, G. C.; Boaz, N. C.; Groves, J. T.; Gunnoe, T. B., Partial oxidation of light alkanes by periodate and

chloride salts. *Dalton Trans.* **2015,** *44* (12), 5294-5298; (d) Fortman, G. C.; Boaz, N. C.; Munz, D.; Konnick, M. M.; Periana, R. A.; Groves, J. T.; Gunnoe, T. B., Selective Monooxidation of Light Alkanes Using Chloride and Iodate. *J. Am. Chem. Soc.* **2014,** *136* (23), 8393-8401. (e) Hirscher, N. A.; Ohri, N.; Yang, Q.; Zhou, J.; Anna, J. M.; Schelter, E. J.; Goldberg, K. I. *J. Am. Chem. Soc.* **2021**, *143*, 19262-19267.
16. (a) Kim, A.-R.; Ahn, S.; Yoon, T.-U.; Notestein, J. M.; Farha, O. K.; Bae, Y.-S., Fast Cyclohexane Oxidation Under Mild Reaction Conditions Through a Controlled Creation of Redox-Active Fe(II/III) Sites in a Metal−Organic Framework. *ChemCatChem* **2019,** *11* (22), 5650-5656; (b) Fahy, K. M.; Liu, A. C.; Barnard, K. R.; Bright, V. R.; Enright, R. J.; Hoggard, P. E., Photooxidation of Cyclohexane by Visible and Near-UV Light Catalyzed by Tetraethylammonium Tetrachloroferrate. *Catalysts* **2018,** *8* (9), 403; (c) Barnard, K. R.; Bright, V. R.; Enright, R. J.; Fahy, K. M.; Liu, A. C.; Hoggard, P. E., Heterogeneous Catalysis by Tetraethylammonium Tetrachloroferrate of the Photooxidation of Toluene by Visible and Near-UV Light. *Catalysts* **2018,** *8* (2), 79.
17. Iranpoor, N.; Adibi, H., Iron(III) trifluoroacetate as an efficient catalyst for solvolytic and nonsolvolytic nucleophilic ring opening of epoxides. *Bull. Chem. Soc. Jpn.* **2000,** *73* (3), 675-680.
18. Guntlin, C. P.; Zund, T.; Kravchyk, K. V.; Worle, M.; Bodnarchuk, M. I.; Kovalenko, M. V., Nanocrystalline FeF_3 and MF_2 (M = Fe, Co, and Mn) from metal trifluoroacetates and their Li(Na)-ion storage properties. *J. Mater. Chem. A* **2017,** *5* (16), 7383-7393.
19. Guntlin, C. P.; Ochsenbein, S. T.; Wörle, M.; Erni, R.; Kravchyk, K. V.; Kovalenko, M. V., Popcorn-Shaped FexO (Wüstite) Nanoparticles from a Single-Source Precursor: Colloidal Synthesis and Magnetic Properties. *Chem. Mater.* **2018,** *30* (4), 1249-1256.
20. Frankiss, S. G., Nuclear Magnetic Reseonance Spectra of Some Substituted Methanes. *J. Phys. Chem.* **1963,** *67* (4), 752-755.
21. Blake, P. G.; Pritchard, H., The thermal decomposition of trifluoroacetic acid. *J. Chem. Soc. B* **1967,** (0), 282-286.
22. Lambert, J. B.; Wang, G. T.; Finzel, R. B.; Teramura, D. H., Stabilization of Positive Charge by Beta-Silicon. *J. Am. Chem. Soc.* **1987,** *109* (25), 7838-7845.

TABLE OF CONTENTS GRAPHIC

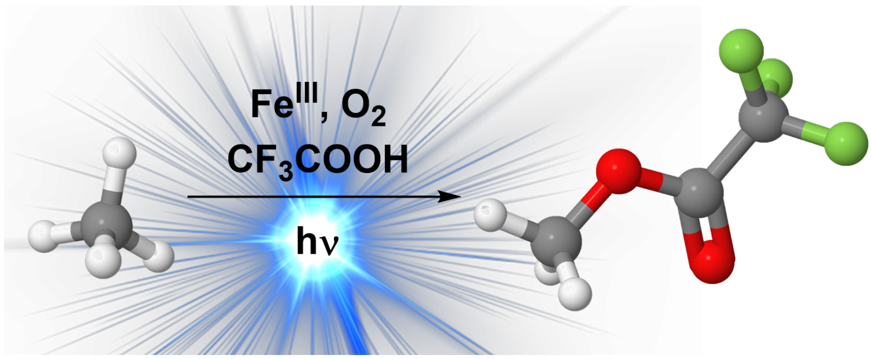

TOC Synopsis

The aerobic oxidation of hydrocarbons, including light alkanes, to generate alkyl esters using an Fe(III) catalyst is described. The reactions produce alkyl esters, occur at ambient temperature in the presence of air, and catalytic turnover is observed for the oxidation of methane in a pure dioxygen atmosphere.